Smoothed Particle Hydrodynamics and its application to the solution of fusion-relevant MHD problems

L.Vela Vela[1,2], R. Sanchez[1], J.M.Reynolds-Barredo[1], J.Geiger[2]

[1] *Universidad Carlos III, Leganés, Spain*

[2] *Max-Planck Institute for Plasma Physics, Greifswald, Germany*

The present study is motivated by the lack of tools to study the stability properties of plasma configurations that include magnetic islands and stochastic regions. These equilibrium solutions do not assume the existence of nested closed magnetic surfaces and can not be easily tackled analytically, instead codes like SIESTA [1] construct them numerically. Wendelstein 7-X depends on our capabilities to keep the X-points of its islands and the divertors aligned, hence the pressing need to understand the stability properties of such configurations.

In astrophysics, a Lagrangian numerical method designed to solve the equation son hydrodynamics is commonly used to simulate galaxy dynamics, and astrophysical plasmas in general. The method is called Smoothed Particle Hydrodynamics (SPH) and was first introduced in the 70's by Gingold and Monaghan [2] together with Lucy [3]. In SPH all fields are "carried by the particles" and are evaluated via interpolation formulas, in contrast to what is done in other methods such as particle-in-cell (PIC) codes. This interpolation procedure allows us to discretise the spatial derivatives on a co-moving frame and to obtain evolution equations for the particle's position, velocity, mass density, internal energy and magnetic field.

$$\rho_a = \sum_b m_b W_{ab}(H_a) \tag{1}$$

$$\frac{dv_a^i}{dt} = -\sum_b m_b \left(\frac{\mathbb{S}_a}{\Omega_a \rho_a^2} F_{ab}(H_a) + \frac{\mathbb{S}_b}{\Omega_b \rho_b^2} F_{ab}(H_b) \right) \cdot \mathbf{r}_{ab} \tag{2}$$

$$\frac{dB_a^i}{dt} = -\sum_b m_b \left(\mathbf{B}_a (\mathbf{v}_{ab} \cdot \mathbf{r}_{ab}) - \mathbf{v}_{ab} (\mathbf{B}_a \cdot \mathbf{r}_{ab}) \right) \frac{F_{ab}(H_a)}{\rho_a \Omega_a} \tag{3}$$

$$\frac{du_a}{dt} = -\frac{p_a}{\rho_a} \sum_b m_b (\mathbf{v}_{ab} \cdot \mathbf{r}_{ab}) \frac{F_{ab}(H_a)}{\rho_a \Omega_a} \tag{4}$$

The evolution equations of the system (eqs.1, 2, 3 and 4)[1] are constructed by identifying the Lagrangian function of the system, and minimising the corresponding action functional [4].

[1]Here, W is the interpolating kernel, usually a bell-shaped, gaussian like function. The notation $\mathbf{r}_{ab}$ is shorthanded for $\mathbf{r}_a - \mathbf{r}_b$ and similarly for the velocity and the magnetic field. $W_{ab} = W(|\mathbf{r}_{ab}|)$ and its gradient is given by: $\nabla W_{ab} = -\mathbf{r}_{ab} F_{ab}$. The factor Ω must be included to account for a spatially varying smoothing lengths H. Finally, the tensor $\mathbb{S}$ is given by $-(p + B^2/2\mu_0)\mathbb{I} + \mathbf{BB}/\mu_0$

The resulting equation of motion has very desirable conservation properties (mass, momentum, angular momentum and energy) hard-wired into it. In order to use SPH to simulate the temporal evolution of MHD systems with fusion-relevant geometries however, we must first overcome to following two challenges:

1.) *Use ghost particles to enforce boundary conditions near smoothly curved walls*. Using ghost particles around flat walls is common use in SPH, however, the inclusion of curved walls complicates the matter. To solve it, we proceed by expressing the position of the ghost particle corresponding to particle a, that is a', in terms of the known position $\mathbf{r}_a$ via the map $\mathbf{r}_{a'} = \psi(\mathbf{r}_a)$ where the map has to fulfil the following differential equation:

$$\boxed{\frac{\partial \psi}{\partial s} = -\frac{\mathbf{J}(s)}{\mathbf{J}(\psi(s))}} \qquad \text{with} \qquad \psi(\mathbf{r_a}) = \mathbf{r}_a \; \forall \; \mathbf{r}_a \text{ at the boundary} \tag{5}$$

where $\mathbf{J}$ is the Jacobian of the transformation between carteian coordinates $\{x,y,z\}$ and a suitable set of coordinates $\{s,u,v\}$. The map ψ can be solved exactly for circles, spheres, cylinders and tori by choosing $\{s,u,v\}$ to be the usual polar, spherical, cylindrical, and toroidal coordinates. Once the exact solution for the 2D circle in known, every 2D curve can be locally approximated with a circle of radius $1/\kappa$ where κ is its local curvature. This opens the possibility of using the ghost particle approach in SPH with any domain with curved walls.

2.) *Replicate arbitrary initial conditions with high-fidelity.*

This challenge comes from our need to replicate rigorously, and down to the last detail, the equilibrium states of SIESTA and VMEC to later study its stability properties. There are good reasons [5] why to use equal masses for every SPH particle, hence the problem is not trivial (See eq.1). In fact, this is an inverse problem where the positions of the particles have to be found so as to give rise to the right mass density.

The ALARIC algorithm [6] was developed to combine well-behaved relaxation techniques with faster and efficient concepts from multi-grid methods. ALARIC made possible the creation of arbitrarily complex density profiles with an exceptionally low level of noise. The low levels of numerical noise are crucial to the study of stability properties of a system since high-fidelity temporal evolution of small perturbations is possible. Fig.1 shows the temporal evolution of the noise level in the initial density profile as a function of the elapsed time-steps. We see how ALARIC delivers better results in a reasonable amount of time.

Solving the two previous challenges allows us to consider cylindrical geometries of relevance to fusion. As a first example, a theta-pinch has been initialised with the equilibrium profiles listed in [7]. Using the Energy Principle we determine that any small perturbation to this system will have a positive growth rate irregardless of the perturbation, hence the system is stable.

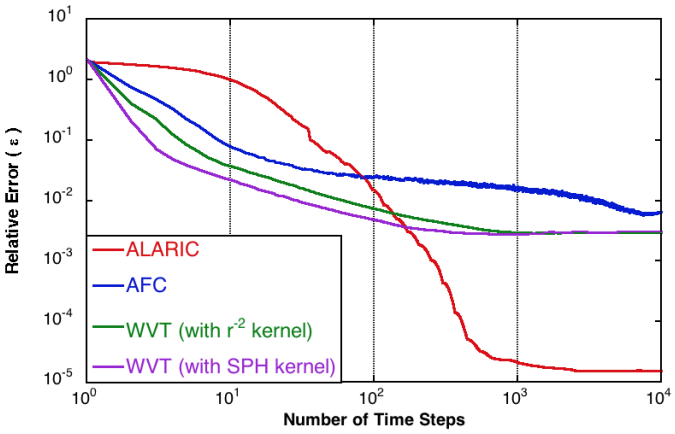

Figure 1: *Initial condition error as function of required time-steps. ALARIC delivers solutions 2 orders of magnitude better, in only 1 order of magnitude more time-steps.*

Our results are illustrated in fig.2 where the final snapshot (at $t = 7t_A$) of the theta pinch radial profiles (left) and the constant pressure iso-surfaces of the plasma column (right) are shown. We can see how the profiles have remain unchanged, and the plasma column remains perfectly flat. In contrast, fig.3 shows a Zeta pinch after a similar period of time. The Zeta pinch is predicted to be always unstable against the $m = 1$ kink modes according to the Energy principle [7]. We can see how the radial profiles, initially a thin line, become noisy. The reason behind this can be easily understood by looking at the rightmost part of fig.3 where the kink instability is visible, and the horizontal displacement of the column displacement will cause any the radial projection to become noisy.

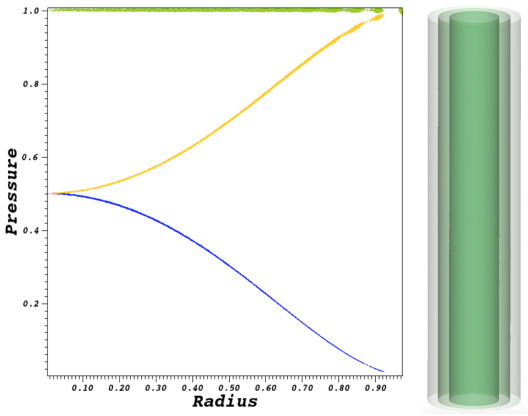

Figure 2: *Theta Pinch final snapshot*

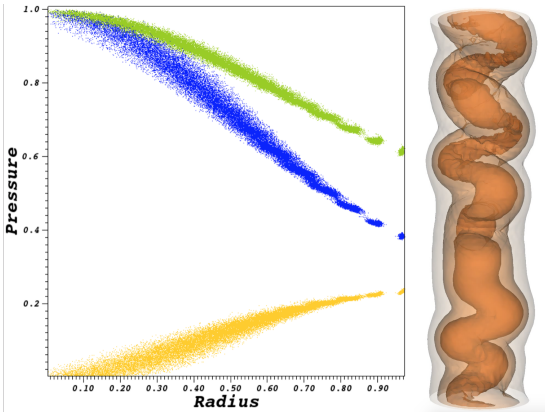

Figure 3: *Zeta Pinch final snapshot*

Last, we include resistive dynamics in our SPH implementation. The extension of the usual MHD equations consist of the two following terms:

$$\left.\frac{d\mathbf{B}}{dt}\right|_\eta = \eta\nabla^2\mathbf{B} + \mathscr{S} \qquad \left.\frac{du}{dt}\right|_\eta = \eta j^2 \tag{6}$$

where $\mathscr{S}$ is an artificial source term needed to sustain the equilibrium in the presence of resistivity [8]. As a test, we construct a force-free scenario where the evolution of the magnetic energy can be modelled analytically. Fig.4 shows the dissipation rate of the magnetic energy as a function of the wave number of the initial profile. We see how for small wave numbers, the agreement is perfect however, above a certain wave number, the dissipation rate seems to saturate. This is because our system can only resolve up to a certain wave number.

In green and purple lines, fig.4 shows the maximum wave number that can still be properly sampled (4 particles/period) and the Nyquist sampling rate (2 particles/period) respectively. The correct implementation of resistive dynamics in the SPH equations allows us to tackle problems of magnetic reconnection like the Harris current-sheet problem where a island is expected to form within the domain with an O-point in the upper half of the plane, and a reconnection X-point in the lower. Fig.5 shows the magnetic field lines after the island has finally opened up. The position of the O and X points agrees with the model.

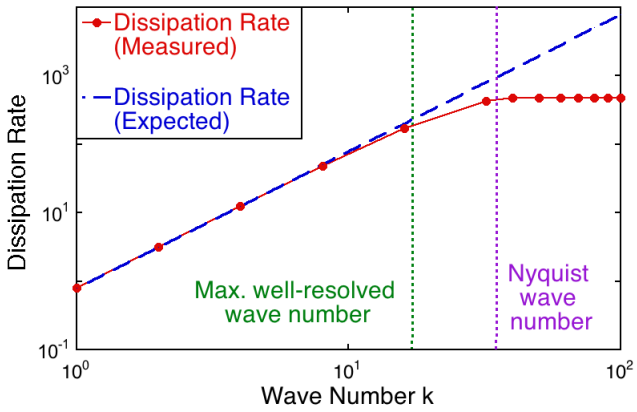

Figure 4: *Dissipation rate as a function of the wave-number of the system. For well-resolved scenarios the agreement is perfect, while for scenarios with less than two-particles per wavelength (Nyquist wave number) the dissipation saturates.*

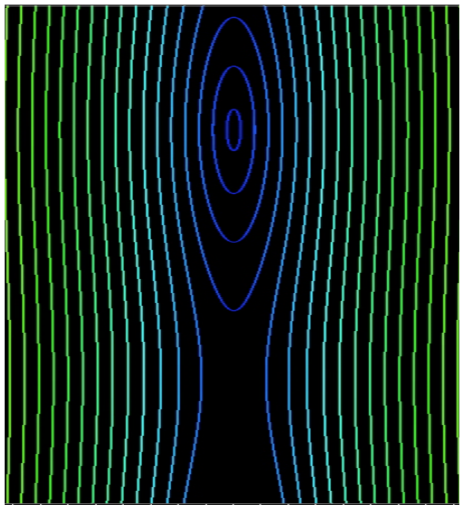

Figure 5: *Island opening in the* $\mathbf{j} \times \mathbf{B} = 0$ *version of the Harris current sheet test.*

References

[1] S. Hirshman, R. Sanchez, and C. Cook *PoP*, vol. 18, no. 6, p. 062504, 2011.

[2] R. A. Gingold and J. J. Monaghan *Monthly notices RAS*, vol. 181, no. 3, pp. 375–389, 1977.

[3] L. B. Lucy *TAJ*, vol. 82, pp. 1013–1024, 1977.

[4] D. J. Price *JCP*, vol. 231, no. 3, pp. 759–794, 2012.

[5] M. Herant *Memorie della SAI*, vol. 65, p. 1013, 1994.

[6] L. V. Vela, R. Sanchez, and J. Geiger *CPC*, 2017.

[7] J. P. Freidberg. CUP, 2014.

[8] D. Knoll and L. Chacón *PRL*, vol. 88, no. 21, p. 215003, 2002.